Published in final edited form as:
Mol Phys. 2013 April 1; 111(7): 922–929. doi:10.1080/00268976.2012.758324.

A Euclidean Perspective on the Unfolding of Azurin: Spatial Correlations

Jeffrey J. Warren[†], **Harry B. Gray**[†], **Jay R. Winkler**[†], and **John J. Kozak**[‡,*]
[†]Beckman Institute, California Institute of Technology, Pasadena CA 91125
[‡]DePaul University, 243 South Wabash Ave., Chicago, IL 60604-8875

Abstract

We investigate the stability to structural perturbation of *Pseudomonas aeruginosa* azurin using a previously developed geometric model. Our analysis considers Ru(2,2′,6′,2″-terpyridine)(1,10-phenanthroline)(His83)-labeled wild-type azurin and five variants with mutations to Cu-ligating residues. We find that in the early stages of unfolding, the β-strands exhibit the most structural stability. The conserved residues comprising the hydrophobic core are dislocated only after nearly complete unfolding of the β-barrel. Attachment of the Ru-complex at His83 does not destabilize the protein fold, despite causing some degree of structural rearrangement. Notably, replacing the Cys112 and/or Met121 Cu ligands does not affect the conformational integrity of the protein. Notably, these results are in accord with experimental evidence, as well as molecular dynamics simulations of the denaturation of azurin.

Keywords

Azurin; protein folding; modeling

1. Introduction

Pseudomonas aeruginosa azurin continues to play a key role in investigations of electron transfer processes and energy transduction pathways in proteins [1,2]. It also is serving as a model in studies that probe whether the folding of small proteins occurs via a hierarchical or nonhierarchical mechanism [3–12]. In a hierarchical mechanism, native-like secondary structures form rapidly, interacting with each other to produce intermediates of ever-increasing complexity, ultimately yielding the native configuration. Alternatively, in a nonhierarchical mechanism, folding can be envisioned as a two-state process with no transitory, intermediate states. Distinguishing between these two possibilities is experimentally difficult because the intermediates are typically short-lived and weakly interacting. In an alternative approach, some workers are focusing on early stages in the denaturation of a protein, arguing that unfolding is the reverse of folding [13–18]. In this light, we have developed a simple geometrical model that describes the initial stages of unfolding.

We consider Ru(2,2′,6′,2″-terpyridine)(1,10-phenanthroline)(His83)-labeled azurin [made from wild-type (WT) azurin] and five variants in which the Cu-ligating 112 (Cys) and 121 (Met) residues are replaced with other amino acids. All of the azurins considered are in the

kozak@depaul.edu.

Supplementary Content Available Online
Complete unfolding metrics for all azurins studied.

oxidized (Cu^{II}) form. While engineered mutants can reduce the stability of the proteins, many mutations tend not to affect *global* folding [18–21]. In fact, in a study on WT azurin, Manetto *et al.* [18] demonstrated that removal of residues 54–67 encompassing the α-helix leaves the β-barrel essentially intact. Here, we document and compare the stability of the six azurin variants to structural perturbation in the early stages of denaturation and compare our results to molecular dynamics simulations and experiment for unfolding/folding of WT protein.

We proceed using the crystallographic data for a given protein and calculate the distance of the α-carbon of each residue from the Cu ion (the origin of our coordinate system) [22–24]. Keeping the geometry of each triad of n = 3 residues invariant (specified by the crystallographic data), we consider a sequence of evolving states in which two triads (n = 5 residues), three triads (n = 7 residues), and so on, up to seven triads (n = 15 residues), are aligned in a maximally extended configuration. We then calculate the displacement of the α-carbon of the central residue in each of these extended configurations from Cu and construct the ratio $\mathbf{S_i}$ of this new distance to the corresponding distance in the native state. Calculations are carried out for all 128 residues of each azurin variant and, taken together, provide a global perspective on the early stages in the denaturation. Our model is aimed at providing a very inexpensive way to survey protein features that could play prominent roles in folding/unfolding; and such an approach may facilitate more detailed, dynamical calculations.

Our approach is based on two geometric theorems, the Law of Cosines, which follows from propositions II.12 and II.13 in Euclid's *Elements* (ca. 300 BC) and the Law of Sines, which was known to and used by Ptolemy (ca. 200 AD). Importantly, once the geometrical model is formulated, no further approximations are introduced and the results presented here are limited only by the accuracy of the coordinates from the crystallographic structures. The present study focuses on the spatial displacement of residues and regions of azurin as it unfolds and provides tests of the robustness of our model, as well as comparisons to experimental and other theoretical approaches.

2. Methods

Calculations were carried out using a model introduced in our earlier work and applied previously to several proteins [20–22]. To implement our approach for azurin, the only inputs are the crystallographic coordinates for each α-carbon in the peptide backbone. The objective is to calculate the change in distance of the α-carbon of each azurin residue from a common reference point, specified to be the position of the Cu ion, as the protein unfolds. In carrying out this calculation, we impose the constraint that the geometry of each triad of n = 3 residues, specified by the crystallographic data, remains invariant. We then consider sequentially a series of evolving states in which two triads (n = 5 residues), three (n = 7 residues), four (n = 9 residues), five (n = 11 residues), six (n = 13 residues), and seven triads (n = 15 residues), are aligned in a maximally extended, linear configuration. The displacement from the Cu ion of the α-carbon of the central residue in each of these extended configurations is determined and a ratio of this new distance to the corresponding distance in the native state is calculated. The analysis of the quantitative changes in values of these ratios ($\mathbf{S_i}$) is the basis for the conclusions in this study.

To provide a specific example of the calculational procedure, consider the segment of the polypeptide chain between residue R_{01} and residue R_{07} in azurin, diagrammed schematically in Figure 1; the midpoint residue is R_{04} in this example. Relative to the Cu ion, the distance (in Å) to the residue R_{01} ($D(Cu - R_{01})$) and to the residue R_{07} ($D(Cu - R_{07})$) can be calculated from the crystallographic data using the theorem of Pythagoras:

$$D(\mathrm{Cu}-R_{01})=\sqrt{(R_{01,x}-\mathrm{Cu}_x)^2+(R_{01,y}-\mathrm{Cu}_y)^2+(R_{01,z}-\mathrm{Cu}_z)^2}=28.54\ \text{Å} \quad (1)$$

$$D(\mathrm{Cu}-R_{07})=\sqrt{(R_{07,x}-\mathrm{Cu}_x)^2+(R_{07,y}-\mathrm{Cu}_y)^2+(R_{07,z}-\mathrm{Cu}_z)^2}=12.23\ \text{Å} \quad (2)$$

Therefore:

$$D(R_{01}-R_{07})=\sqrt{(R_{01,x}-R_{07,x})^2+(R_{01,y}-R_{07,y})^2+(R_{01,z}-R_{07,z})^2}=17.70\ \text{Å} \quad (3)$$

where $\{Cu_x, Cu_y, Cu_z\}$, $\{R_{01,x}, R_{01,y}, R_{01,z}\}$ and $\{R_{07,x}, R_{07,y}, R_{07,z}\}$ are the crystallographic coordinates for Cu, and the α carbons of residues 1 and 7, respectively.

When azurin begins to unfold, the polypeptide chain becomes more extended; one possible configuration is the maximally extended state, illustrated at the top of Figure 1. The triplet distances $S(R_{01} – R_{03})$, $S(R_{03} – R_{05})$ and $S(R_{05} – R_{07})$ in the native (folded) state also can be calculated from the crystallographic data using the Pythagorean theorem:

$$S(R_{01}-R_{03})=\sqrt{(R_{03,x}-R_{01,x})^2+(R_{03,y}-R_{01,y})^2+(R_{03,z}-R_{01,z})^2}=5.95\ \text{Å} \quad (4)$$

$$S(R_{03}-R_{05})=\sqrt{(R_{05,x}-R_{03,x})^2+(R_{05,y}-R_{03,y})^2+(R_{05,z}-R_{03,z})^2}=7.16\ \text{Å} \quad (5)$$

$$S(R_{05}-R_{07})=\sqrt{(R_{07,x}-R_{05,x})^2+(R_{07,y}-R_{05,y})^2+(R_{07,z}-R_{05,z})^2}=6.35\ \text{Å} \quad (6)$$

We define the sum of these three distances as the “fully extended” state, denoted T_{04}:

$$T_{04}=S(R_{01}-R_{03})+S(R_{03}-R_{05})+S(R_{05}-R_{07})=19.45\ \text{Å} \quad (7)$$

We now determine the distance that the midpoint residue R_{04} is displaced as the polypeptide unfolds from the native state to this defined extended state. We first calculate the angle β (Figure 1) using the Law of Cosines: in a triangle with angles α, β and γ and sides opposite a, b and c, respectively,

$$c^2=a^2+b^2-2ab\cos(\beta) \quad (8)$$

where $a = D(Cu – R_{01}) = 28.54$ Å, $b = D(Cu – R_{07}) = 12.23$ Å and $c = D(R_{01} – R_{07}) = 17.70$ Å. Solving for cos β yields cos β = 0.9318 and β= 21.3°. Similarly, the angles opposite the sides $a = D(Cu – R_{01})$ and $b = D(Cu – R_{07})$ (α and γ respectively) have the values α = 144.2° and γ = 14.5°. The angles α, β and γ sum to 180°, as they must.

To complete the calculation of the extension ratio $\mathbf{S_i}$, we use the Law of Sines:

$$\frac{a}{\sin\alpha}=\frac{b}{\sin\beta}=\frac{c}{\sin\gamma} \quad (9)$$

If $\rho = D(Cu - R_{04})$ is the distance between the Cu ion and the residue R_{04} in the native state, we assign $\rho' = D(Cu - R_{04})'$ to be the distance between the Cu ion and the residue R_{04} in the fully extended state (Figure 1). From the Law of Sines:

$$\frac{T_{04}}{\sin\beta} = \frac{\rho'}{\sin\alpha} \quad (10)$$

Since T_{04}, α and β are known, ρ' can be determined; $\rho' = 31.64$ Å. Finally, given $y = \rho \sin\alpha$ and $y' = a\rho' \sin\alpha$ we have $y'/y = \rho'/\rho = \mathbf{S_i} = 1.099$

The same calculations, which were carried out for each of the 128 residues for each azurin variant, for each of the extended states, n = 5 to 15, provide a global perspective on the early stages of denaturation. We also can group protein structures (e.g. β-barrels) to gain insight into how discrete protein structures begin to unfold. Once the geometrical model is formulated, no further approximations are introduced and the results are limited only by the accuracy of the crystallographic coordinates. This approach is based entirely on the Pythagorean theorem and, the Law of Cosines and the Law of Sines.

3. Results

3.1 Primary and Secondary Structure of Azurin

The present study is based on the crystallographic data for Ru(His83)-labeled azurin (azurin A) and five variants (Table 1) [25,26]. Note that differences occur only at the 112 and 121 positions, which are Cu-coordinating residues, and the two entries, E7 and E9, refer to the same azurin variant at pH 7 and 9, respectively. Scheme 1 designates the principal components of the *secondary* structure. For later reference, the distance in Ångstroms of each residue from the Cu ion is specified in under each entry. Azurins are highly structured proteins, with nearly 60% of the residues belonging to an α-helical or β-strand segment.

3.2 Early Stages in the Unfolding of Helical Regions

An α-helical region is determined from crystallographic data via an algorithm that specifies the beginning and end of the region by plus or minus one residue. Taking the above uncertainty into account, we distinguished the behavior of “internal” residues in an α-helix from residues on the boundary of a turning region. As shown in [24], the resiliency to steric perturbation of the internal residues in all α-helices reported for the five proteins considered (cyt *c*, cb_{562}, cyt c', azurin and lysozyme) is remarkably similar.

The longest α-helical region in azurin comprises residues 55–67. Further, we define the nine residues, 57–65, as the internal residues for this helical region ($\mathbf{H_2}$). A benchmark based on the unfolding behavior of $\mathbf{H_2}$ is used below to compare and contrast the unfolding of other regions of the polypeptide chain. In our model, the coordinates of each triad of n = 3 residues are fixed by the native state geometry, so the value of the ratio $\mathbf{S_i}$ for this configuration is 1. As the protein unfolds, the value of the ratio $\mathbf{S_i}$ will change. To characterize the unfolding of the internal residues in the helical region $\mathbf{H_2}$, we calculate (for each setting of n) the average value $\langle \mathbf{S_{av}} \rangle$ for the nine internal residues, 57–65 (Table 2). For unfolded states following the completion of a full turn of the α-helix, there is near uniformity in values of the average $\langle S_{av} \rangle$. This uniformity is observed for the proteins in our earlier work [24]. Also noteworthy is the nearly uniform, but smaller, value of $\langle \mathbf{S_{av}} \rangle$ for the n = 7 extension, a value that also characterizes the case n = 7 for all proteins studied previously. Considering the complete data set on all the azurin variants for the extensions n = 5, 9, and 11, an overall average can be determined, $\langle \mathbf{S_{av}} \rangle = 1.77$ (with variance 0.0005 and standard deviation 0.0230). This value provides a benchmark against which the

unfolding behavior of individual residues and other regions of the polypeptide chain can be assessed, as described below.

We next consider the unfolding of β-sheet residues in the six azurins. The $<\mathbf{S_{av}}>$ values set out in Table 3 are for all residues in the given β-strand for azurin A. Data for all other azurins are similar (Table S3). The specific averages calculated for the extension metric $<\mathbf{S_{av}}>$ are remarkably constant across all the variants. Since our geometrical model requires a minimum of 5 residues to carry out the extension calculation, a full data set can only be provided for the β-strand residues comprising **S2**, **S3**, **S4**, **S6** and **S7**. Only the first one or two extensions can be assessed for the near-terminal β-sheet residues specified by **S1** and **S8**, and none for **S5**.

The resiliency of the β-barrel is evident. Through the extensions n = 5, 7, 9 and 11, the stability of residues comprising all β–strands is greater than that characterizing $\mathbf{H_2}$. This greater resiliency persists for all β-strands except **S4** through the extension n = 13. Only when we consider the maximal extension (here) of n = 15 residues do we find two β-strands, **S2** and **S4**, that are more labile than the internal residues comprising the α-helix $\mathbf{H_2}$ (the β-strands **S3**, **S6** and **S7** maintain their near native-state topology until completely extended).

The β-barrel of azurin is built around a hydrophobic core of eight conserved hydrophobic residues: Val31, Leu33, Trp48, Leu50, Val95, Phe97, Tyr108, and Phe110 [27]. Comparing the stability of these residues versus $\mathbf{H_2}$, the values of $\mathbf{S_i}$ for each residue (Table 4) show that Val31, Leu33, Val95, and Phe97 are as stable to geometric perturbation as β-strand residues and much more stable than internal residues in the α-helix $\mathbf{H_2}$. The residues Trp48, Tyr108 and Phe110 are of stability similar to the internal residues in the α-helix $\mathbf{H_2}$; only Leu50 is more labile.

The disulfide bond between Cys3 and Cys26 provides additional, non-nearest-neighbor stabilization of the native structure. In our model, the disulfide is ruptured almost immediately upon steric perturbation; already for n = 7, $\mathbf{S_{26}}$ is larger than 2. Disulfide rupture is not expected to occur without reduction, which our model does not account for. Azurins without the Cys3-Cys26 disulfide unfold much more easily than WT azurin [28], but their x-ray structures are superimposable with those of azurins with intact disulfides [29]. As such, our model is still applicable in the case of azurin, but it is not necessarily applicable to other proteins that contain disulfides.

3.3 Metal Atom Coordinating Residues

Five residues coordinate the Cu ion in azurin at the “north” pole of the β-barrel. The key residues are His46, His117, and Cys112, which are in a trigonal configuration. The Cu ion also weakly interacts with the thioether of Met121 and the carbonyl oxygen of Gly45. The engineered residues are X_1112 (X_1 = Cys, Asp) and X_2121 (X_2 = Met, Phe, Ile, Leu, Glu) (Table 1). The engineered azurins exhibit the same unfolding history for these residues as for azurin A (see Supporting Information). Considered individually, the residues Gly 45, His46 and X_2121 have a stability to steric perturbation comparable to residues in the most resilient β-strands; the X_1112 is somewhat more labile, comparable to the internal residues in the α-helix $\mathbf{H_2}$. Only His117 is more labile than either helical regime, but significantly so. The Cu ligand His117 is surface exposed with no hydrogen bonds to peripheral residues [26], so it is likely that (similar to surface atoms in a crystal) the absence of boundary constraints permits the outward extension of the segment of the polypeptide chain containing it.

3.4 Unfolding of Boundary Regions

We showed previously that residues flanking the boundary of an α-helical region have differential susceptibility to steric perturbation of the α-helix [23,24]. The discrimination may be different for the two boundary regions bracketing a given α-helix, as well as between or among the boundary regions for different α-helices in a given protein (e.g. unfolding of four-bundle cytochromes [23,24]). The data for azurin A (Table 5) and all variants studied (Table S2) are averages calculated using the residue specific values of $\mathbf{S_i}$ for four residues: two residues preceding the onset of a helical region and the first two residues defining that helical region. In these tables, we use the notation $\mathbf{H_i(l)}$ to denote the four-residue boundary region at the left of helix $\mathbf{H_i}$, and $\mathbf{H_i(r)}$ to denote the one to the right. We find that even under the most strenuous steric perturbation, the case n = 15, the boundary regions $\mathbf{H_1(r)}$, $\mathbf{H_4(l)}$ and $\mathbf{H_5(r)}$ (the latter region housing Met121) have stabilities similar to $\mathbf{H_2}$. However, the five boundary regions $\mathbf{H_1(l)}$, $\mathbf{H_2(l)}$, $\mathbf{H_3(r)}$, $\mathbf{H_4(r)}$, and $\mathbf{H_5(l)}$ are significantly more sensitive to structural perturbation.

4. Discussion

The unfolding metrics described above provide a picture of azurin unfolding. The progression of unfolding of the structured regions is given in Table 6. We also can calculate the positions for each residue for each unfolding metric. We show the results for n = 5 and n = 15 with respect to the native structure of the protein in Figures 2 and 3, respectively. To summarize, th main α-helix, smaller helicies and turning regions begin to unfold early (n = 5), while the hydrophobic core remains largely intact through n = 15, which is roughly equivalent to a nearly denatured state. This unfolding profile is, in some ways, a reflection of the inherent flexibility of regions of the protein; and in this regard it is similar to molecular dynamics (MD) simulations of the structural flexibility of the macromolecule [30].

We observe that up to the extended state involving n = 13 residues, the structural stability of β-strands is greater than that exhibited by the nine internal residues in the α-helix $\mathbf{H}_2$. This conclusion is consistent with high-temperature molecular dynamics (MD) simulations by Rizzuti *et al.* who concluded that unfolding of the β-barrel is associated with dislocation of the main α-helix [16]. Whereas our geometrical approach offers snapshots along the initial unfolding pathway, the dynamical simulations provide evidence for the “flapping” of the α-helix with respect to the rest of the protein. MD simulations [16] also reveal that in the first stages of unfolding, the β-barrel is largely unperturbed, also consistent with our results. Our data show (Table 6) that there is essentially no disruption of the β-topology through the first two stages of unfolding. We also observe that $\mathbf{S_4}$, at the N-terminal side of $\mathbf{H_2}$, is more susceptible to unfolding than the other strands in the β-barrel, again in accord with MD simulations [16].

Our calculations indicate that values of $\mathbf{S_i}$ for the conserved hydrophobic residues Val31, Leu33, Val95, and Phe97 are less sensitive to geometric perturbation than the $\langle \mathbf{S_{av}} \rangle$ values $\mathbf{H_2}$; the residues Trp48, Tyr108 and Phe110 are of stability similar to the internal residues in $\mathbf{H_2}$; only Leu50 is somewhat more labile than the internal residues in α-helix $\mathbf{H_2}$. These observations are again in agreement with MD simulations [16]. We conclude that Val31, Leu33, Val95 and Phe97 (and probably Trp48, Tyr108 and Phe110) are dislocated only after unfolding of the β-barrel. Kinetics analysis of folding of site-directed variants suggests that Val31, Leu33, Leu50, and Val95 form native-like interactions that contribute to formation of the native state, while Trp48 and Phe110 stabilize the folded protein [31].

Investigations of the structure and dynamics of Trp48 during azurin unfolding using a host of spectroscopic techniques reveal that exposure of this residue is an early event [15].

Likewise, MD simulations show that separation of the α-helix from the rest of the protein causes Trp48 to pull away from the still folded β-barrel [16]. We reach the equivalent conclusion that the apparent separation of Trp48 (Table 4) from the β-strand **S5** (Table 5) first becomes noticeable after n = 7, and then dramatically so when subject to the further structural perturbations imposed by residue extensions n = 9 through n = 15.

The α-helices in all azurins show an invariance of $<\mathbf{S_{av}}>$ (1.77) for extensions larger than n = 5 (Table 5). Interestingly, $<\mathbf{S_{av}}>$ also is the same as for internal residues in the helices of the other proteins we have analyzed (wild type azurin, cyt *c*, cb_{562}, cyt c' and lysozyme) [24]. The natural question is: Why should there be a universal plateau of $<\mathbf{S_i}>$ for such different proteins? It was noted that α-helices invariably have 3.6 residues per turn, giving them a stable structure, but also provide some flexibility [32]. Since all α-helices show this behavior, then $<\mathbf{S_{av}}>$ will always plateau after a linear extension of n = 5 residues, i.e., following one turn of the α-helix. The spirit of our model, as well was that in [32], goes back to the seminal contributions of Ramachandran *et al.* [33], who used crystallographic coordinates to identify two dihedral angles (φ,ψ) flanking each peptide bond, and constructed [φ, ψ] plots for all residues in a given protein. In [32], emphasis is placed on angular "twist" of the α-helix, and in our model we shift emphasis to the spatial distance of the metal ion in the protein to the α-carbon of each residue.

Assuming that the folding and unfolding pathways are the same, tracking our calculation in reverse order, i.e., going from n = 15 to n = 3, provides insight into the folding of azurin. Our data show that coalescence of the conserved hydrophobic core is realized first, followed by the emergence of the β-strand scaffolding and then, finally, the alignment and attachment of the 13-residue α-helix to the β-scaffolding. Given this scenario, it would be of interest to attempt to reconcile our results with predictions of a sequential collapse model [34,35].

We note that in the context of our model that all six azurin variants studied here, as well as the WT protein [24], behave similarly. The effect of pH (E7 versus E9) is negligible, as is the presence of a Ru-photolabel, even though it causes some structural modification in surrounding loop regions. The protein structures are nearly superimposable, so the close agreement in results is not surprising for our geometrical model. Nonetheless, it is comforting that minor perturbations in x-ray structures do not drastically affect the predictions derived from the geometrical model.

4.1 Implications and Limitations

The most noteworthy aspect of our geometrical unfolding model is that, despite its striking simplicity, it compares very favorably with the general conclusions from computationally more expensive models. Notably, it identifies regions and discrete residues that have been experimentally and computationally shown to be important features in protein stability and unfolding/folding. Although our purely geometrical model is a valuable starting point, it cannot compete with molecular dynamics and Monte Carlo simulations if the goal is to capture the main features of unfolding or folding dynamics.

A key limitation is that our model does not explicitly consider linkages between residues, like disulfides. The disulfide bond is substantially stronger than the hydrogen bonding and hydrophobic interactions that hold proteins together. Extra care should be taken in applying this model to systems with disulfides, or other cross-linked cofactors that derive from the protein backbone (e.g. the Tyr-His pair in cytochrome *c* oxidase [36]).

We should emphasize that, because our purely geometrical model is not based on physical phenomena like H-bonding or hydrophobic interactions, β-sheets in azurin are predicted to almost invariably unfold after α-helices because they already are in a more extended state.

Moreover, we are limited by crystallographic coordinates, which can only provide snapshots of the states of a protein. Again, critical assessment of the results from our model is necessary before making firm conclusions. Despite these potential shortcomings, our model faithfully reproduces the folding/unfolding features for azurin and the relative stabilities of 4-helix bundle cytochromes c' and cb_{562} [23].

5. Conclusion

We have extended our geometrical model for predicting early stages of protein unfolding to six azurin variants, including some with variations in the Cu active site. The close agreement between results for the six variants attests to the robustness of the model. In sum, the results show that the main azurin α-helix and turning regions are the most susceptible to unfolding, while the main β-barrel and hydrophobic core are the most resistant, in accord with experiments and calculations. Our approach is quite distinct from other computational methods, but reveals many of the same features of unfolding for azurin. We suggest that our model provides an elegantly simple way to chart the initial stages of protein unfolding. We are currently extending our model to include angular correlations of protein substructures as unfolding progresses.

Supplementary Material

Refer to Web version on PubMed Central for supplementary material.

Acknowledgments

Work at Caltech was supported by NIH (GM095037 to JJW, DK019038 to HBG and GM068461 to JRW).

References

1. Gray HB, Malmström BG, Williams RJP. J Biol Inorg Chem. 2000; 5:551. [PubMed: 11085645]
2. Dennison C. Coord Chem Rev. 2005; 249:3025.
3. Jackson SE. Folding Des. 1998; 3:R81.
4. Baldwin RL, Rose GD. Trends Biochem Sci. 1999; 24:26. [PubMed: 10087919]
5. Baldwin RL, Rose GD. Trends Biochem Sci. 1999; 24:77. [PubMed: 10098403]
6. Eaton WA, Muñoz V, Hagen SJ, Jas GS, Lapidus LJ, Henry ER, Hofrichter J. Annu Rev Biophys Biomol Struct. 2000; 29:327. [PubMed: 10940252]
7. Fersht AR. Proc Natl Acad Sci USA. 2000; 97:1525. [PubMed: 10677494]
8. Finkelstein AV, Galzitskaya OV. Phys Life Rev. 2004; 1:23.
9. Kamagata K, Arai M, Kuwajima K. J Mol Biol. 2004; 339:951. [PubMed: 15165862]
10. Ivankov DN, Finkelstein AV. Proc Natl Acad Sci USA. 2004; 101:8942. [PubMed: 15184682]
11. Maity H, Maity M, Krishna MMG, Mayne L, Englander SW. Proc Natl Acad Sci USA. 2005; 102:4741. [PubMed: 15774579]
12. Feng H, Zhou Z, Bai Y. Proc Natl Acad Sci USA. 2005; 102:5026. [PubMed: 15793003]
13. Lazaridis T, Karplus M. Science. 1997; 278:1928. [PubMed: 9395391]
14. La Rosa C, Milardi D, Grasso D, Guzzi R, Sportelli L. J Phys Chem. 1995; 99:14864.
15. Guzzi R, La Rosa C, Grasso D, Milardi D, Sportelli L. Biophys Chem. 1996; 60:29.
16. Rizzuti B, Daggett V, Guzzi R, Sportelli L. Biochemistry. 2004; 43:15601.
17. Rizzuti B, Swart M, Sportelli L, Guzzi R. J Mol Model. 2004; 10:25. [PubMed: 14691672]
18. Manetto GD, Grasso DM, Milardi D, Pappalardo M, Guzzi R, Sportelli L, Verbeet MP, Canters GW, La Rosa C. ChemBioChem. 2007; 8:1941. [PubMed: 17868155]
19. Mizoguchi TJ, Di Bilio AJ, Gray HB, Richards JH. J Am Chem Soc. 1992; 114:10076.

20. Lancaster KM, George SD, Yokoyama K, Richards JH, Gray HB. Nat Chem. 2009; 1:711. [PubMed: 20305734]
21. Li C, Sato K, Monari S, Salard I, Sola M, Banfield MJ, Dennison C. Inorg Chem. 2010; 50:482.
22. Urie KG, Pletneva E, Gray HB, Winkler JR, Kozak JJ. Mol Phys. 2011; 109:301. [PubMed: 21379364]
23. Gray HB, Winkler JR, Kozak JJ. Mol Phys. 2011; 109:905.
24. Gray HB, Winkler JR, Kozak JJ. Mol Phys. 2012; 110:419.
25. Lancaster KM, Sproules S, Palmer JH, Richards JH, Gray HB. J Am Chem Soc. 2010; 132:14590. [PubMed: 20879734]
26. Crane BR, Di Bilio AJ, Winkler JR, Gray HB. J Am Chem Soc. 2001; 123:11623. [PubMed: 11716717]
27. Engman KC, Sandberg A, Leckner J, Karlsson BG. Protein Sci. 2004; 13:2706. [PubMed: 15340166]
28. Guzzi R, Sportelli L, La Rosa C, Milardi D, Grasso D, Verbeet MP, Canters GW. Biophys J. 1999; 77:1052. [PubMed: 10423449]
29. Bonander N, Leckner J, Guo H, Karlsson BG, Sjölin L. Eur J Biochem. 2000; 267:4511. [PubMed: 10880975]
30. Arcangeli C, Bizzarri AR, Cannistraro S. Biophys Chem. 1999; 78:247. [PubMed: 17030312]
31. Wilson CJ, Wittung-Stafshede P. Proc Natl Acad Sci USA. 2005; 102:3984. [PubMed: 15753320]
32. Ackbarow T, Chen X, Keten S, Buehler MJ. Proc Natl Acad Sci USA. 2007; 104:16410. [PubMed: 17925444]
33. Ramachandran GN, Ramakrishnan C, Sasisekharan V. J Mol Biol. 1963; 7:95. [PubMed: 13990617]
34. Bergasa-Caceres F, Ronneberg TA, Rabitz HA. J Phys Chem B. 1999; 103:9749.
35. Bergasa-Caceres F, Rabitz HA. J Phys Chem B. 2003; 107:12874.
36. Kaila VRI, Verkhovsky MI, Wikström M. Chem Rev. 2010; 110:7062. [PubMed: 21053971]

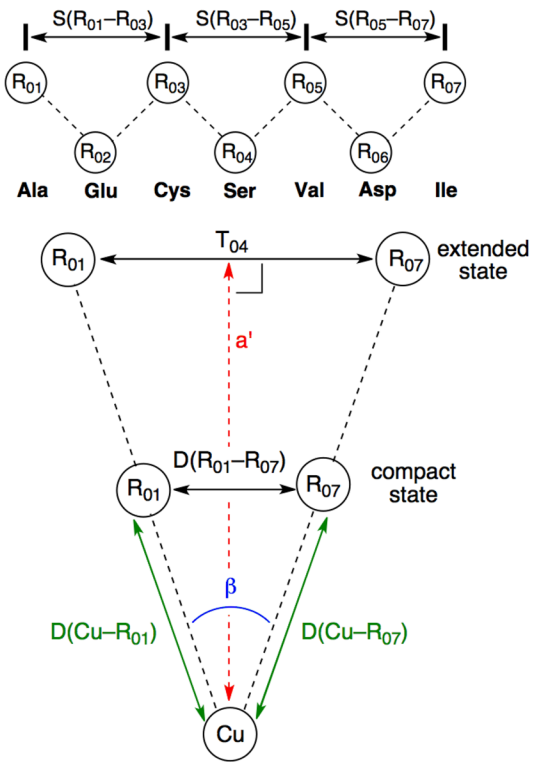

Figure 1.
Schematic description of the geometric protein unfolding model, using azurin as an example. The top most configuration shows our definition of the fully extended state.

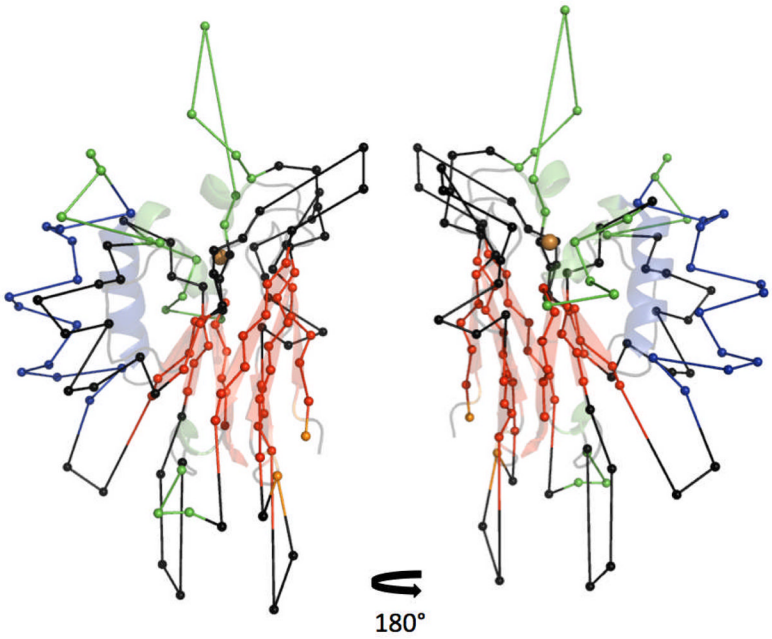

Figure 2.
Calculated displacement of Cα for azurin A (n = 5 unfolding metric) The native structure is shown with a partially transparent ribbon diagram. Color coding as in Scheme 1.

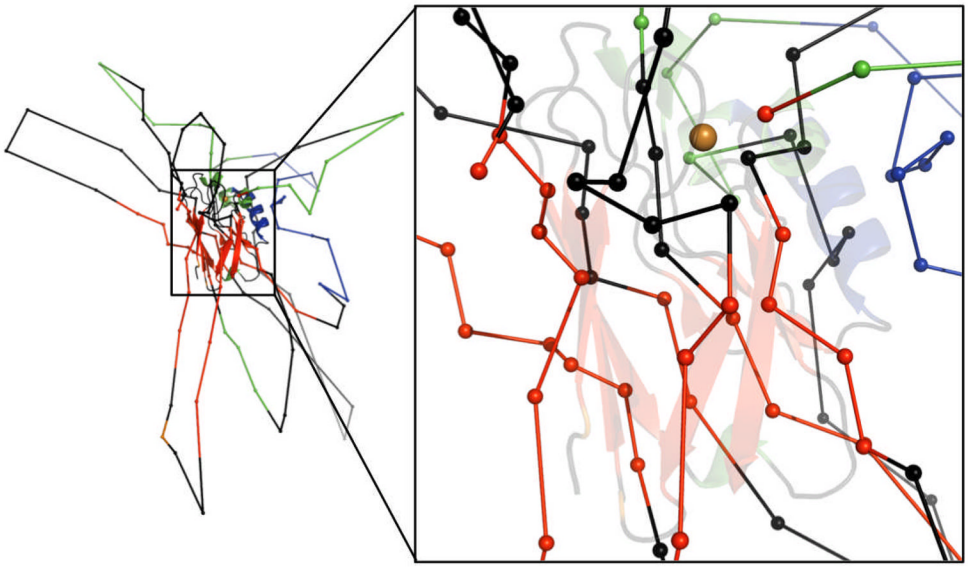

Figure 3.
Calculated displacement of Cα for azurin A (n = 15 unfolding metric). The native structure is shown with a partially transparent ribbon diagram. Color coding as in Scheme 1.

1	ALA	GLU	CYS	SER	VAL	ASP	ILE	GLN	GLY	ASN	ASP	GLN	MET	GLN	PHE	ASN	THR
	28.5	25.2	23.6	20.5	17.7	15.8	12.2	10.3	6.8	8.1	8.8	9.6	6.1	7.6	8.5	12.2	13.6
18	ASN	ALA	ILE	THR	VAL	ASP	LYS	SER	CYS	LYS	GLN	PHE	THR	VAL	ASN	LEU	SER
	14.1	16.5	17.5	21.2	22.4	26.1	28.4	30.3	27.4	27.9	24.5	21.3	19.0	15.4	14.8	11.3	11.2
35	HIS	PRO	GLY	ASN	LEU	PRO	LYS	ASN	VAL	MET	GLY	HIS	ASN	TRP	VAL	LEU	SER
	9.6	12.2	11.1	13.0	10.9	10.8	8.4	9.9	8.9	5.8	4.9	3.4	6.0	8.3	10.2	13.5	15.9
52	THR	ALA	ALA	ASP	MET	GLN	GLY	VAL	VAL	THR	ASP	GLY	MET	ALA	SER	GLY	LEU
	18.6	18.0	20.1	18.1	14.6	15.3	16.7	14.0	11.3	14.0	15.3	12.0	11.3	14.9	13.3	11.7	14.8
69	ASP	LYS	ASP	TYR	LEU	LYS	PRO	ASP	ASP	SER	ARG	VAL	ILE	ALA	HIS	THR	LYS
	14.8	14.2	10.7	10.0	12.3	15.9	18.3	20.1	18.5	20.8	18.8	16.2	17.9	16.0	12.7	11.6	11.0
86	LEU	ILE	GLY	SER	GLY	GLU	LYS	ASP	SER	VAL	THR	PHE	ASP	VAL	SER	LYS	LEU
	8.0	8.5	9.0	11.2	14.0	13.0	13.1	13.5	15.4	16.3	19.6	20.8	24.1	24.4	26.9	24.2	23.8
103	LYS	GLU	GLY	GLU	GLN	TYR	MET	PHE	PHE	CYS	THR	PHE	PRO	GLY	HIS	SER	ALA
	26.5	27.7	27.7	24.6	21.3	18.1	14.5	11.5	4.7	4.7	6.3	4.9	7.6	8.0	4.9	7.2	9.7
120	LEU	MET	LYS	GLY	THR	LEU	THR	LEU	LYS								
	9.0	6.6	9.5	12.8	16.1	17.6	21.3	24.2	27.0								

Scheme 1.

Sequence and secondary structure for azurin A. The α-helix (54–67) is coded in blue and shorter helical segments in green. β-sheet residues are shown in red. Disulfide Cys are in orange. Distances (Å) of the α-carbon of each residue from Cu are listed below each residue.

Table 1

Abbreviations and residue differences among azurin variants.

	A [26]	D [19b]	F [19b]	I [19b]	L [19b]	E7 [25]	E9 [25]
PDB ID	1JZF	3FQY	3FQ2	3FQ1	3FPY	3NP3	3NP4
Resolution (Å)	1.50	1.90	1.91	1.90	2.10	2.10	2.25
Residue 112	Cys	Asp	Asp	Asp	Asp	Asp	Asp
Residue 121	Met	Met	Phe	Ile	Leu	Glu	Glu

Table 2

<S_{av}> for unfolding of α-helical region H_2 in six azurin variants.

	A	D	F	I	L	E7	E9
3	1.00	1.00	1.00	1.00	1.00	1.00	1.00
1 turn (3.6 residues)							
5	1.76	1.79	1.77	1.77	1.78	1.77	1.77
7	1.63	1.65	1.64	1.65	1.64	1.64	1.64
2 turns (7.2 residues)							
9	1.78	1.81	1.80	1.80	1.79	1.79	1.78
3 turns (10.8 residues)							
11	1.73	1.76	1.75	1.75	1.74	1.74	1.74
13	1.74	1.75	1.75	1.76	1.73	1.72	1.73
4 turns (14.4 residues)							

Mol Phys. Author manuscript; available in PMC 2014 April 01.

Table 3

Comparison of <S_i> for β-strand unfolding in azurin A variants.[a]

metric	5	7	9	11	13	15
S1: Ser4 Val5 Asp6 Ile7 Gln8; <R> = 15.3 Å						
	1.04	1.05	--	--	--	--
S2: Ala19 Ile20 Thr21 Val22 Asp23; <R> = 20.7 Å						
	1.03	1.15	1.19	1.34	1.62	1.94
S3: Gln28 Phe29 Thr30 Val31 Asn32 Leu33 Ser34; <R> = 16.8 Å						
	1.04	1.06	1.09	1.19	1.33	1.50
S4: Val49 Leu50 Ser51 Thr52; <R> = 14.6 Å						
	1.06	1.25	1.48	1.68	1.87	2.18
S6: Lys92 Asp93 Ser94 Val95 Thr96 Phe97 Asp98 Val99; <R> = 17.5 Å						
	1.01	1.07	1.15	1.28	1.42	1.65
S7: Tyr108 Met109 Phe110 Phe111; <R> 13.0 Å						
	1.03	1.05	1.09	1.23	1.42	1.73
S8: Lys122 Gly123 Thr124 Leu125 Thr126 Leu127 Lys128; <R> = 18.4						
	1.04	--	--	--	--	--

[a] <**R**> is the mean distance from Cu to the residues comprising the β-strand.

Table 4

<S_i> conserved hydrophobic residues in six azurin variants[a]

metric	5	7	9	11	13	15
Val31 (**S3**); R = 15.38 Å						
	1.00	1.01	1.00	1.13	1.15	1.21
Leu33 (**S3**); R = 11.26 Å						
	1.01	1.02	1.01	1.05	1.09	1.33
Trp48; R = 8.28 Å						
	1.04	1.05	1.12	1.24	1.39	1.77
Leu50 (**S4**) R = 13.51 Å						
	1.03	1.14	1.22	1.48	1.91	2.04
Val95 (**S6**) R = 13.51 Å						
	1.00	1.01	1.05	1.04	1.24	1.57
Phe97 (**S6**) R = 20.81 Å						
	1.05	1.03	1.23	1.28	1.25	1.28
Tyr108 (**S7**) R = 18.31 Å						
	1.00	1.02	1.12	1.41	1.61	1.72
Phe110 (**S7**) R = 11.47 Å						
	1.03	1.08	1.06	1.10	1.29	1.67

[a]R is the distance of the residue from Cu. The β-sheet location is denoted $\mathbf{S_n}$.

Table 5

$\langle S_i \rangle$ for unfolding of boundary regions in azurin A.

metric	3	7	9	11	13	15
H_1(l): Asn38 Leu39 Pro40 Lys41						
	1.34	1.71	2.05	2.66	3.36	4.08
H_1(r): Met44 Gly45 His46 Asn47						
	1.10	1.32	1.36	1.42	1.46	1.55
H_2(l): Ala53 Ala54 Asp55 Met56						
	1.60	1.81	2.17	2.54	2.74	3.16
H_3(r): Lys70 Asp71 Tyr72 Leu73						
	1.51	1.77	2.36	2.20	2.37	3.10
H_4(l): Asp98 Val99 Ser100 Lys101						
	1.32	1.32	1.32	1.37	1.53	1.76
H_4(r): Lys101 Leu102 Lys103 Glu104						
	1.32	1.38	1.60	1.91	2.29	2.80
H_5(l): Phe114 Pro115 Gly116 His117						
	1.49	2.19	2.64	3.69	4.50	5.37
H_5(r): Ala119 Leu120 Met121 Lys122						
	1.60	1.43	1.39	1.42	1.61	1.61

Table 6

Unfolding metrics <$\mathbf{S_{av}}$> for structured regions in azurin A.[a]

***n* = 5**	***n* = 9**	***n* =13**	***n* =15**
S1	S1	S1	S1
S2	*S2*	*S2*	**S2**
S3	*S3*	*S3*	*S3*
H1(l)	**H1(l)**	**H1(l)**	**H1(l)**
H1(r)	*H1(r)*	*H1(r)*	*H1(r)*
S4	*S4*	*S4*	**S4**
H2(l)	**H2(l)**	**H2(l)**	**H2(l)**
H2	H2	H2	H2
H3(r)	**H3(r)**	**H3(r)**	**H3(r)**
S6	*S6*	*S6*	*S6*
H4(r)	*H4(r)*	**H4(r)**	**H4(r)**
S7	*S7*	*S7*	*S7*
H5(l)	**H5(l)**	**H5(l)**	**H5(l)**
H(5)r	*H(5)r*	*H(5)r*	*H(5)r*
S8	S8	S8	S8

[a]The main α-helical region is H_2. Regions more labile than H_2 in bold, regions less labile in italic and regions that are similarly labile are in normal font.